Hut-shaped lead nanowires with one-dimensional electronic properties

M. Kopciuszyński [●],[*] A. Stępniak-Dybala [●], M. Dachniewicz, L. Żurawek [●], M. Krawiec [●], and R. Zdyb [●]
Institute of Physics, Maria Curie-Sklodowska University, Pl. M. Curie-Skłodowskiej 1, PL-20-031 Lublin, Poland

The ultrathin Pb layer on the Si(110) surface might be converted into hut-shaped nanowires extending in a unique [$\bar{1}$10] direction. Despite the fact that about 2.6 ML of lead is used to form an ordered array of nanowires, this system shows not only anisotropy of the electronic structure but also a small band gap in the [001] direction. Among several quasi-one-dimensional bands, two of them show pure one-dimensional character. Electron dispersion maps measured with photoelectron spectroscopy are supported by scanning tunneling spectroscopy data which confirm the absence of electronic states at the Fermi level in areas between lead nanowires. Based on first-principles density functional theory calculations four different structural models of lead nanowires are proposed reflecting a different number of Pb atoms in the unit cell.

I. INTRODUCTION

The interaction between lead atoms and silicon substrate was investigated for several decades. The most intense study were carried out on the Si(111) surface [1,2]. Depending on the amount of Pb deposited onto the Si(111) in the range between 1.2 ML and 1.33 ML the mixture of $\sqrt{3}\times\sqrt{7}$ and $\sqrt{3}\times\sqrt{3}$ superstructure forms the Devil's staircase phase diagram [3,4]. Both superstructures, as well as their mixture, show metallic bands in the electronic structure with parabolic dispersion [5]. If lead is deposited at about 200 K the amorphous wetting layer is formed that remains stable to a critical coverage about 1.22 ML. When this amount is exceeded, lead forms perfect crystalline, uniform *magic height* islands [6–8]. This process is extremely fast and it is called *explosive* nucleation [8].

The question arises if those phenomena observed in two-dimensional (2D) Pb layer manifest themselves also on narrow terraces—quasi-one-dimensional (1D) system. This idea was realized for the first time on a vicinal Si(557) surface [9]. This system might be indeed switched between 1D and 2D conductivity depending on its temperature [9,10]. However, the electronic structure measured at 70 K shows rather 2D character with only 1D modulation [11]. Further investigation confirmed 2D electronic coupling in the Si(557)-Pb system and the 1D conductivity was assigned to the periodic self-organization of Pb chains [12,13]. Lead atoms form similar nanostructures on the Si(553) substrate [14], but as it was recently proven, the electronic structure is radically different and features purely 1D bands [15]. Moreover, studies on another example, namely the Si(113)-Pb surface, shows that lead forms partly embedded chains but still with 1D electronic properties [16,17]. For higher amount of lead deposited onto anisotropic surfaces: Si(100), Si(335), Si(557), and Si(110), it forms mesoscopic nanocrystals with lateral size in the range of 50 nm that extends along the [$\bar{1}$10] direction [18].

Such variety of electronic and structural properties of lead 1D nanostructures is intriguing. There is also a whole family of 1D gold chains grown on vicinal substrates: Si(335) [19,20], Si(553) [20–26], Si(557) [27–29], Si(775) [20,30] as well as anisotropic (5×2)-Au reconstruction formed on flat Si(111) surface [28,31,32]. All those chain structures show 1D electronic bands with parabolic dispersion along the [$\bar{1}$10] direction.

Si(110) surface provides a bridge between flat (111) and stepped vicinal silicon surfaces. It may be considered as the extreme case of vicinal surface with terraces of $1\frac{1}{3}\times a^{\mathrm{Si}}_{[11\bar{2}]}$ width (where $a^{\mathrm{Si}}_{[11\bar{2}]} = 3.325$ Å) as well as relatively flat surface with rectangular symmetry that makes it a desirable substrate which may promote the growth of 1D nanostructures. Several chain structures could be formed on the Si(110) using materials like: gold [33,34], platinum [35,36], or lead which forms also (7×2), (1×1) superstructures [37,38].

In this paper we demonstrate the formation of hut-shaped nanowires on Si(110) surface and study their structural and electronic properties. The crystallographic structure was investigated by scanning tunneling microscopy (STM). The electronic structure was determined by angle-resolved photoelectron spectroscopy (ARPES) and scanning tunneling spectroscopy (STS). We propose four different structural models of the prepared 1D nanostructures based on first-principle calculations.

II. METHODS

The measurements were performed in three different ultrahigh vacuum (UHV) chambers (base pressure in the middle of 10^{-11} mbar range) each equipped with a lead effusion cell, quartz microbalance, and reflection high energy electron diffraction (RHEED). The quartz microbalance has been calibrated during layer-by-layer growth of Pb on the Si(111)-(6×6)Au surface at 130 K [39]. One monolayer of Pb (ML) refers to the density of atoms in bulk terminated Si(110) layer considering only one atom per unit cell

[*]m.kopciuszynski@umcs.pl

(one sublattice of the diamond structure) which gives the value of 4.80×10^{14} atoms/cm^2.

The Si(110)-Pb sample was prepared by deposition of about 3 ML of Pb on a clean Si(110) surface and subsequent annealing at 530 K for several minutes. Detailed preparation procedure was described in our previous work [40].

STM and STS results were obtained with Omicron VT and LT STM operating at room temperature as well as at 4.5 K. Both tungsten electrochemical etched and platinum iridium tips were used. The scanning tunneling spectroscopy was done at room temperature simultaneously with topography measurements. One line of $I(V)$ curves acquisition was done every few lines of topography scans. The feedback loop was switched on between and off during $I(V)$ scans. The setpoint was -0.8 V and 500 pA. The dI/dV curves were normalized and calculated numerically.

The ARPES measurements have been performed with helium lamp (unpolarized HeI line, $h\nu = 21.2$ eV) and hemispherical electron energy analyzer (Specs Phoibos 150) with MCP electron detector. The angular and energy multidetection as well as sample rotation were applied to obtain two wave vector components together with binding energy. The ARPES measurements were done at 130 K sample temperature. The energy and angular resolutions were set to 30 meV and $0.25°$, respectively.

First-principles density functional theory calculations were performed within Perdew-Burke-Ernzerhof (PBE) [41] generalized gradient approximation (GGA) to the exchange-correlation interaction, as implemented in VASP (Vienna *ab initio* simulation package) [42,43]. The core electrons were treated within the projector-augmented wave method [44]. The plane-wave energy cutoff for all calculations was set to 340 eV. The convergence criterion of total energy for self-consistent field calculations was chosen to be 10^{-6} eV. The Brillouin zone was sampled by a $9 \times 3 \times 1$ Monkhorst-Pack k-points grid including the Γ point [45].

The Si(110)-Pb system has been modeled by four double Si layers in Si(110)-(3×1) surface unit cell. The vacuum region as thick as 25 Å has been added to avoid the interaction between surfaces of the slab. All the atomic positions were relaxed by a conjugate gradient method, except the bottom layer, until the largest force in any direction was below 0.01 eV/Å. The Si atoms in the bottom layer were fixed at their bulk positions and saturated by hydrogen atoms. The calculations have been performed with Si-related lattice constant $a_{[\bar{1}10]}^{Si} = 3.87$ Å.

III. RESULTS

A. Crystallographic structure

Figure 1(a) shows an STM image of clean Si(110) surface with (16×2) superstructure. The (16×2) reconstruction forms two domain system with ×2 periodicity extending along two equivalent directions: $[\bar{1}12]$ and $[1\bar{1}2]$ and is well organized only along atomic steps, see the right part of the STM image in Fig. 1(a). It could be obtained over a macroscopic area with significant predominance of one domain orientation if uniform annealing for an extended period of time is applied [46,47]. However, we did not observe any impact
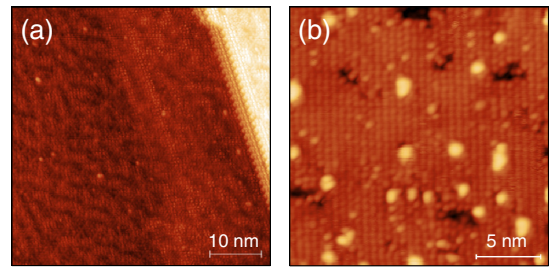

FIG. 1. STM images recorded at 4.5 K of clean Si(110) surface with 16×2 reconstruction ($U = -2$ V, $I = 200$ pA) (a) and covered by 1.1 ML Pb with 1×1, lead induced reconstruction ($U = -1.8$ V, $I = 50$ pA) (b).

of the (16×2) reconstruction quality on the final quality of lead nanostructures. We were able to observe a transitional stage of nanowires growth process that is the formation of Pb induced (1×1) reconstruction. That was visible in STM images recorded after deposition of 1.1 ML Pb and subsequent annealing at 630 K—the temperature close to Pb desorption point, which is shown in Fig. 1(b). The (1×1)-Pb reconstruction was investigated by Kim *et al.* and according to ARPES results it shows semiconducting properties [38]. Several bright features visible in Fig. 1(b) are seeds of lead nanowires.

Figure 2(a) shows the Si(110) surface fully covered by lead nanowires. The periodicity of 16.9 ± 0.5 Å measured across the lead nanostructures on height profile Fig. 2(d) corresponds to three Si lattice constants $3 \times a_{[001]}^{Si}$ Å = 16.29 Å. The height of lead nanostructures is about 1.5 Å. They show triangular cross section that motivated us to name those structures hut-shaped. Two different lattice constants were distinguished in the direction along lead nanowires Figs. 2(e) and 2(f). First, visible on the black profile is equal to 7.6 ± 0.2 Å corresponding to $2 \times a_{[\bar{1}10]}^{Si}$ Å = 7.68 Å. The second one equals to the silicon lattice constant $a_{[\bar{1}10]}^{Si} = 3.84$ Å, and it is visible in the height profile taken from the STM image shown in Fig. 2(b).

The high resolution STM image, Fig. 2(b), was measured in the area marked by the white rectangle in Fig. 2(a) at different bias voltage. Despite the fact that lead nanowires look uniform in larger scale, they differ between each other. For example the wire visible in the middle of Fig. 2(b) is slightly higher than two neighboring wires. It is possible that this particular wire consists of an additional layer of lead atoms which means a larger number of lead atoms per unit cell. Lead nanostructures are not symmetric with respect to the $[\bar{1}10]$ direction, however this could be expected because of the lack of inversion symmetry of the silicon substrate. We were able to observe another feature unique to some nanowires: an additional long distance periodicity (about seven lattice constant) along lead nanostructures which is visible in Fig. 2(c) measured at different bias voltage and confirmed on height profile Fig. 2(g).

Figure 3 shows real and reciprocal lattices of the Si(110) surface with (1×1), (3×1), and (3×2) unit cells marked by red, green, and blue rectangles, respectively. Taking into account the ×3 periodicity observed along the [001] direction and optimal lead coverage that is about 2.6 ML it could be estimated that eight lead atoms fall on the (3×1) unit cell. A
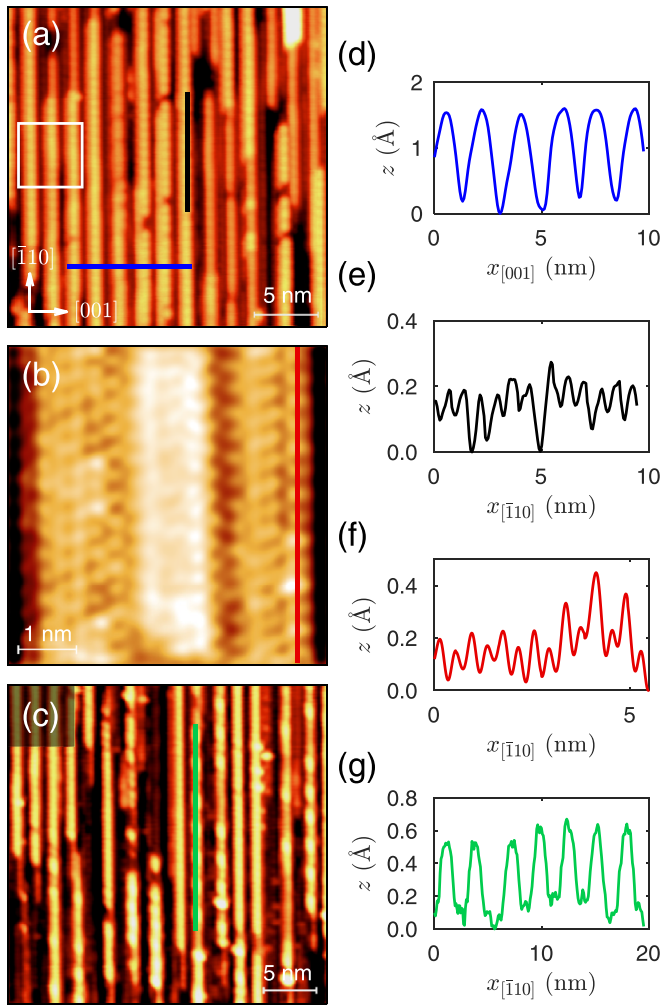
FIG. 2. STM images recorded at 4.5 K of the Si(110)-Pb surface: (a) 25×25 nm^2 area ($U = +1.6$ V, $I = 500$ pA), white rectangle denotes the area that is shown in (b) 5.5×5.5 nm^2 area ($U = -0.5$ V, $I = 600$ pA). (c) STM image showing additional periodicity along some lead nanowires, 30×30 nm^2 area ($U = +0.88$ V, $I = 700$ pA). Height profiles on (d), (e), (f), and (g) were taken along blue, black, red, and green lines marked on STM images.

schematic, hard sphere model of lead hut-shaped nanowires is shown in Fig. 3(b).

B. Electronic structure

Figure 4(a) shows differential conductance map measured on the Si(110)-Pb surface at room temperature. The topography of this particular area is shown in Fig. 4(b). The local density of states (LDOS) is very diverse on the Si(110)-Pb. The highest value of LDOS was measured on the top of lead nanowires and it is almost constant along them. In the areas between the nanowires the LDOS has much lower values.

Figures 4(c) and 4(d) show the dI/dU and normalized $\frac{dI}{dU}/\frac{I}{U}$ curves, respectively. The red curve in Fig. 4(c), recorded on the top of lead nanowire has nonzero value at the Fermi level which means metallic character of this part of lead nanowires, while between them (blue curve) the density of states is suppressed at the Fermi level, that may indicate
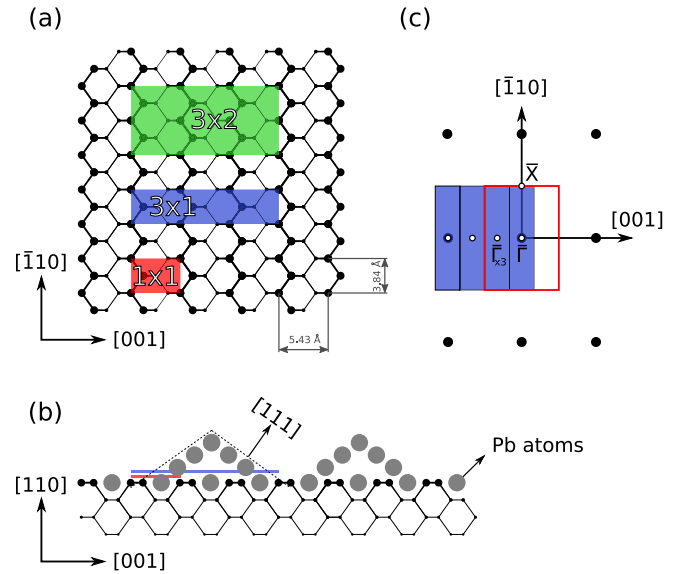

FIG. 3. Sketch showing top (a) and side (b) view of the ball-and-stick model of the Si(110) lattice with three different unit cells: (3×2), (3×1), and (1×1). (c) Reciprocal network with first Brillouin zones of the (3×1)—blue rectangle and (1×1)—red rectangle reconstructed Si(110) surface.

insulating character of the areas between Pb wires. These results suggest one-dimensional character of the Si(110)-Pb surface. Normalized dI/dU curves in Fig. 4(d) show the energy position of electronic states (peaks visible at -0.4 V, $+0.4$ V, and $+0.7$ V).

Figures 5(a) and 5(b) show the electronic structure measured by ARPES along [001] and [$\bar{1}$10] directions, respectively. Those directions may be considered as perpendicular and parallel to the lead nanowires formed on the Si(110) surface and are shown in schematic Fig. 3(c). The $\bar{\Gamma}$ and $_{\times 3}\bar{\Gamma}$ points are marked by white vertical lines. The $_{\times 3}\bar{\Gamma}$ refers to the reciprocal distance in the (3×1) unit cell. Surface Brillouin zones of the (3×1) cell are marked as white rectangles on the constant energy map taken at $E_B = 0$ eV—the Fermi surface, Fig. 5(c).

Four pairs of holelike, parabolic bands are visible in the vicinity of the Fermi level for electronic structure measured along the [001] direction, Fig. 5(a). There is a ×3 band folding in the direction perpendicular to the lead wires that corresponds to their transverse width 3×5.43 Å. The bands measured along [001] are elongated towards the [$\bar{1}$10] direction, which is visible on the constant energy map in Fig. 5(c) (this feature is marked by short red and blue horizontal lines). To explain the origin of those bands the electronic structure was calculated for bulk, (110) terminated silicon substrate. The results are shown as white dashed curves in Fig. 5(a). The overall band shape and position agrees, if ×3 periodicity along the [001] direction is taken into account together with the Rashba type band split of the value $\Delta k = 0.14$ Å^{-1}.

In the direction parallel to lead nanowires, Fig. 5(b), there are several metallic bands with close to parabolic dispersion. Two of them are particularity distinct and are marked by dashed blue and red parabolas in Fig. 5(b). Those bands show pure 1D character that is manifested as two pairs of bright
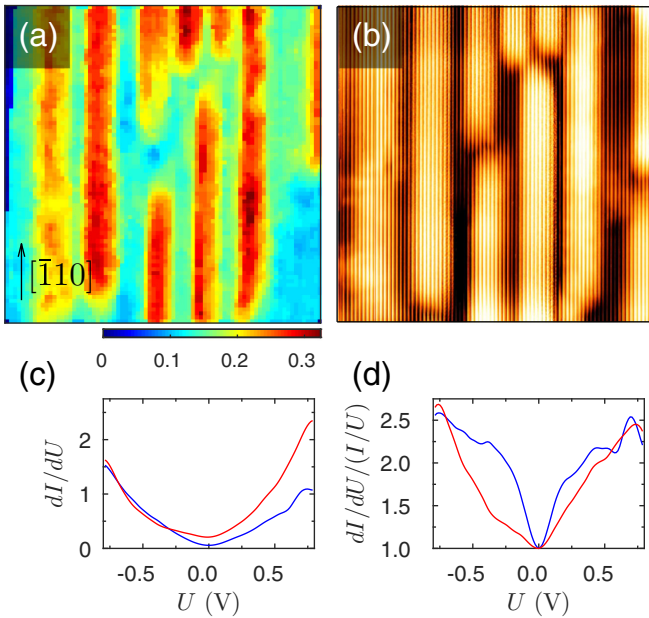
FIG. 4. (a) Differential conductance map measured on the Si(110)-Pb surface at room temperature for 15×15 nm^2 area shown as topography image in (b). STS (scanning tunneling spectroscopy) curves were measured in the range -0.8 to 0.8 V and then used to calculate the first derivative map. Color scale represents the differential conductance in nS at the Fermi level which is proportional to the local density of states. The corresponding topography STM image (b) was measured simultaneously with differential conductance map with the same, reduced space resolution. (c) dI/dU curves obtained on the top of Pb nanowires (red line) and between them (blue line). Both curves are an average of 10 dI/dU curves measured at different points in two areas. (d) Normalized dI/dU curves.

FIG. 5. Electronic structure of the Si(110)-Pb surface measured along two perpendicular directions: [001] (a) and [$\bar{1}$10] (b) (data presented as second derivative maps). (c) Constant energy map taken at 0 eV binding energy—the Fermi surface. Surface Brillouin zones of the 1×3 unit cell are shown as thin, white lines. This map was measured for positive values of wave vector and mirrored according to the surface symmetry. Features marked by white, blue, and red curves on all maps serves as a guide to the eye and are described in text. (d) Integrated energy distribution curves of states in the vicinity of the Fermi level taken from maps measured along [001]—magenta and [$\bar{1}$10]—cyan curve for the wave vector range $0 \div 0.8$ 1/Å.

features on the Fermi surface (marked by vertical, dashed lines) in Fig. 5(c). The Fermi surface is crossed also by a set of bands (three pairs) that show quasi-1D character. Those bands extend along the [001] direction, but they are additionally modulated along [$\bar{1}$10]. As a consequence they show sinusoidal shape on the constant energy map [dotted, white curves in Fig. 5(c)] which suggests an admixture of 2D character.

The electronic structure around the $\bar{\Gamma}$ point consists of two electron bands at the energy 0.15 eV and 0.86 eV. Those relatively flat bands, marked by white, dotted curves in Fig. 5(b) resembles quantum well states that are usually observed in ultrathin lead layers. In fact their position agrees well with the case of three flat lead layers formed on the Si(111) surface [48–50].

The photoelectron intensity measured along the [001] direction in the vicinity of the Fermi level is significantly lower than along the [$\bar{1}$10] direction. The integrated density of states (DOS) curves taken in those two, mutually perpendicular directions suggest that there is a band gap about 15 ± 5 meV in the direction perpendicular to lead nanowires which has been deduced from the shift of two curves in Fig. 5(d) (magenta and cyan curves were integrated along the [001] and [$\bar{1}$10] directions, respectively).

Figure 6 shows photoelectron intensity maps obtained for the direction along the lead nanowires with higher resolution.
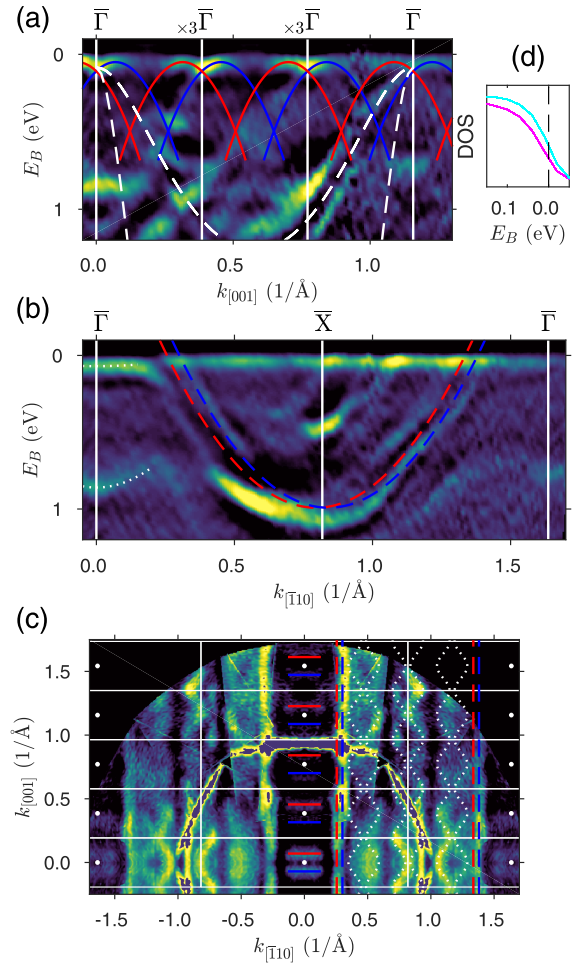
Three maps in Fig. 6(a) present constant energy cuts for binding energies: 0 eV, 0.1 eV, and 0.2 eV. A pair of bands that show pure 1D character appear as straight lines in Fig. 6(a) at $k \sim 0.28$ 1/Å and $k \sim 1.37$ 1/Å and are symmetric in respect to the $\bar{X}_{Si}$ point. Those bands [marked by red and blue dashed parabolas in Figs. 6(b) and 6(c)] have close to parabolic dispersion. The effective electron mass is about $m^* = 0.9 m_e$, where m_e is free-electron mass. The striking similarity between bands marked with blue and red parabolas suggests that this pair is a result of lifted spin degeneracy due to the Rashba-Bychkov effect [51] with $\Delta k = 0.045$ Å^{-1}.

The second group of bands, quasi 1D, shows characteristic sinusoidal shape at the constant energy maps, as mentioned earlier, Fig. 6(a). It is difficult to trace those bands on the dispersion maps and it seems that they obey only partially
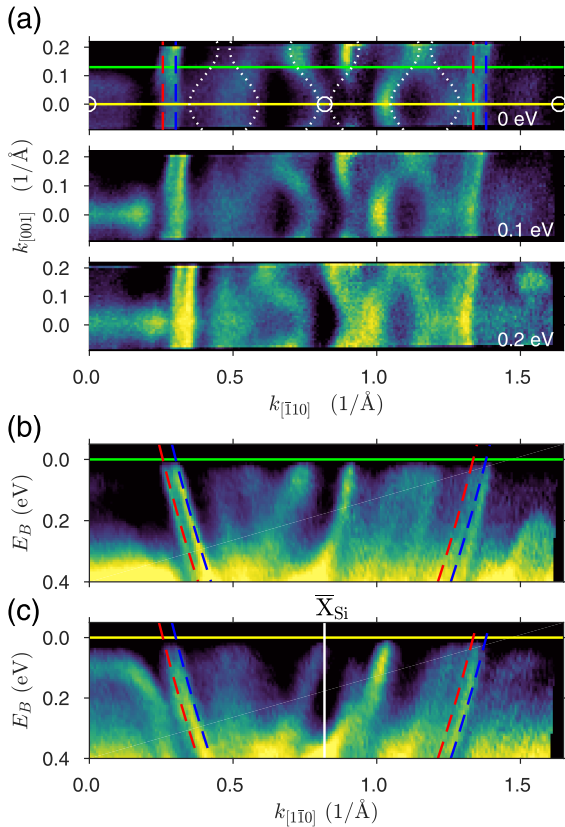
FIG. 6. (a) Constant energy photoemission maps measured with high energy resolution in the vicinity of the Fermi level for binding energies equal to 0, 0.1, and 0.2 eV. (b) and (c) ARPES dispersion maps obtained along green and yellow horizontal lines marked on the Fermi surface (a), respectively. See text for more details.

symmetry rules relative to the $\bar{X}_{Si}$ point. It is possible that matrix elements are smaller or even negligible for some bands which results in lower photoelectron count rate in the ARPES measurements.

C. DFT calculations

Among many tested theoretical models of the Si(110)-Pb calculated for different initial conditions and stoichiometry four were chosen and are presented in Fig. 7. As a starting point the estimated optimal Pb coverage in a range 2.6–2.8 ML as well as the morphology deduced from STM measurements were used. Lead coverage about 2.6 ML suggests that there are about 8–9 Pb atoms per (3×1) Si(110) surface unit cell. However, this estimation is not precise because of two facts: The surface is not perfectly uniform, and additional periodicity ×2 and ×7 or even higher along lead nanowires were also observed. The DFT calculation was performed in the (3×1) unit cell, however (3×2) and (3×3) were also checked. Models D1, D2, D3, and D4 were calculated for 8, 9, 10, and 11 lead atoms per (3×1) unit cell. In all cases, the positions of Si atoms change only slightly, in particular Si dimers become symmetrical.

It is important to note that the results of calculations reproduce the hut-shaped nanowires running along the [$\bar{1}$10] direction for all considered models. Depending on the amount of Pb atoms used in calculations the wires become more and more massive and grow upward forming finally nanowires with triangular cross section (D4). This allows the formation of low index (111) or (100) planes that are energetically favorable.

Despite the assumption based on the STM measurements performed at the early stage of lead nanowires formation (see Fig. 1) it is unclear if the first layer of Pb atoms forms the (1×1) reconstruction. In all structural models lead atoms could be divided into two groups. First, consists of the lowermost, five lead atoms that forms arch shaped ribbon. On top of that ribbon lies three, four, five, or six additional lead atoms (depending on the model) forming a hut shape.

In the third row in Fig. 7 the calculated electronic structure (thin white lines) is superimposed onto the second derivative ARPES maps. It is difficult to identify the best model. For each model the agreement between calculated and measured data is very good at some particular areas of the electronic structure. Those four models calculated for different numbers
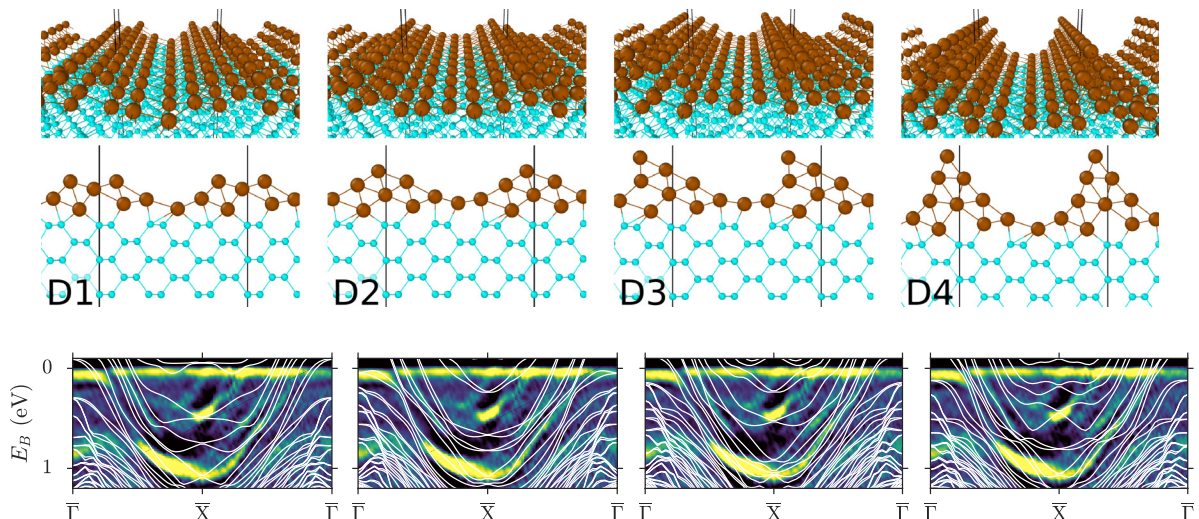

FIG. 7. Four different structural models D1, D2, D3, and D4 with calculated electronic structure superimposed on ARPES data (third row).
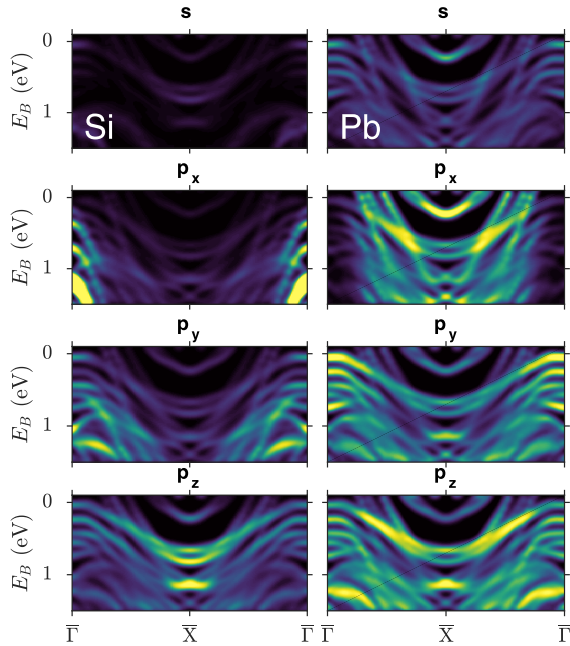
FIG. 8. Theoretical model D2. Relative contribution of different orbitals projected on silicon atoms from the first layer (left column) and all lead atoms forming a nanowire (right column). Data presented as intensity maps.
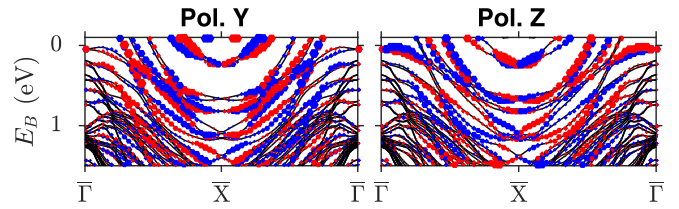

FIG. 9. Theoretical model D2. Spin-polarized band structure projected on different directions of the spin polarizations. Pol. Y and pol. Z correspond to [001] in-plane and [110] out-of-plane directions, respectively. The size of red and blue circles is proportional to the magnitude of spin polarization (only lead atoms were included).

of lead atoms seem to complement each other, and different parts of the band map are well reproduced by different models. That agrees with the conclusion based on the STM results—the surface is composed of several types of lead nanowires.

In all four cases theoretical electronic structure consists of several bands with close to the parabolic dispersion crossing the Fermi level. Models D1 and D2 show only slightly corrugated morphology which agrees with the STM measurements. Those models were calculated for eight and nine lead atoms, respectively, which is the closest value to the estimated number of lead atoms per unit cell.

To determine the origin of metallic bands with parabolic dispersion the contribution of atomic orbitals was checked. Firstly, the lead atoms were divided into several groups. For example, three top lead atoms, three bottom, and the rest of them lying in the middle or five lowermost atoms and the rest of them. However, the contribution of different lead atoms is rather homogeneous. That was another argument to treat lead nanowires as a whole rather than the wetting layer forming (1×1) reconstruction and the rest forming 1D wire.

The normalized contribution of all lead atoms compared with the contribution of silicon atoms located in the first layer of Si(110) substrate are shown as intensity maps in Fig. 8. Data presented in successive rows apply to s, p_x, p_y, p_z orbitals. In general, the contribution of Si atoms to the paraboliclike bands is negligible (see left column in Fig. 8). Both silicon and lead atoms show high p_z and significant p_y contribution for relatively flat, parabolic band, close to the $\overline{X}$ point, at about 0.6 eV binding energy. This suggests the hybridization between both subsystems. The parabolic bands crossing the Fermi level have dominant p_x character and originate from Pb atoms forming nanowires. Those orbitals are

aligned along the $[\bar{1}10]$ which is another argument for the 1D character.

Figure 9 shows the spin-polarized band structure projected on different directions of the spin polarization. For the y and z components a significant spin polarization is visible for most of the electronic bands. This is an indirect argument that a pair of parabolic bands with pure 1D character (Fig. 6) might be spin polarized. There is no spin polarization projected on the x axis due to the symmetry along the $[\bar{1}10]$ direction (results not shown here).

IV. DISCUSSION

Lead can form one-dimensional structures on Si(557) [9,12,52], Si(553) [14,15,53], and Si(113) [17]. There is one striking similarity between reported Si(110)-Pb structure and lead on Si(557) and Si(553). In those cases the transverse width of lead nanowires is equal to: $4\frac{2}{3} \times a_{[11\bar{2}]}^{\mathrm{Si}} = 15.5$ Å, $4\frac{1}{3} \times a_{[11\bar{2}]}^{\mathrm{Si}} = 14.4$ Å, and $3 \times a_{[001]}^{\mathrm{Si}} = 16.3$ Å for the Si(557) switched into (223) and (111) facet structure [52,54]; Si(553) and Si(110), respectively. Only in the case of Si(553) the preferred width is consistent with substrate geometry—it is the width of the (553) silicon terraces [14].

In those three cases the number of lead atoms in the direction perpendicular to the nanowire is equal to 4 on Si(557) [10], 5 on Si(553) [15], and 5 on Si(110) taking into account only the first layer of lead atoms. This suggests that these systems may manifest a *magic width*, an analogy to *magic height* equal to 7 ML observed when lead forms nanocrystals on the Si(111) surface [6–8]. Thus, it would mean a preferred lateral size of lead nanostructures.

Another structural feature is periodic modulation observed for some lead wires with the size of 7 silicon lattice constant. This is similar to the case of Si(553)-Pb [14], however in the latter, the ×7 period was observed on the whole surface, not only for particular chains and bias voltages. The same is true for Si(557)-Pb where ×10 period is manifested [10,55]. The present case, due to the STM bias-dependent periodicity, suggests rather charge density wave behavior. Moreover, the ×7 period along lead wires is not the only one observed in the measurements [see Fig. 2(c)]. The incommensurability between lead and silicon lattice constants might produce different phases of lead wires in a similar way to Devil's staircase phase diagram observed on the Si(111) surface [3].

In our previous work, Ref. [40], it was reported that diffraction measurements (RHEED) show lead bulk lattice constant

along the [$\bar{1}10$] direction: $a^{Pb}_{[\bar{1}10]} = 3.50$ Å. It was suggested that on the top of the nanowire lead atoms preserve bulk lattice constant and may form commensurate phase where 12 lead lattice match 11 silicon lattice constants. However, this conclusion was not confirmed by STM measurements [40] and it seems untrue by the current high resolution STM measurements performed at 4.5 K. It is possible that bulk Pb lattice constant visible in the RHEED patterns (in Ref. [40]) was associated with massive lead wires that might be formed in larger scale.

Despite the similarities between Si(557)-Pb and Si(553)-Pb to the reported here Si(110)-Pb it must be remembered that in the latter case the lead wires are not flat in atomic scale. They show triangular cross section and very likely form low index planes. In fact the lead nanowires resembles mesoscopic, massive wires formed on: Si(100), Si(335), Si(557), and Si(110) [18]. Those massive wires could be obtained at about 5 ML Pb coverage on the surface pre-ordered by Au deposition [18]. While these structures are many times larger (lateral width in the range 500 Å) their cross section is also triangular that is a consequence of the formation of low index (111) and (100) lead planes. This suggests that the reported case could be considered as nanoscopic version of such massive wires.

An unresolved structural issue is the presence of (1×1) lead wetting layer beneath the wires. Measurements done at early stages of the Si(110)-Pb preparation suggest that the (1×1) might serve as foundation for the lead nanowires. This layer might facilitate the lead transport in similar way that is observed during lead nanocrystal growth on the Si(111) [8]. However, in contrast to the striped incommensurate-Pb phase on the Si(111), which is metallic and even superconducting at low temperatures [56,57], the Si(110)-(1×1)-Pb shows semiconducting properties [38] that support 1D electronic properties of the reported nanostructures.

The electronic structure of the Si(110)-Pb system is very similar to that measured for lead nanoribbons formed on the Si(553) surface [15]. In both cases there are several bands crossing the Fermi level with close to parabolic dispersion along the [$\bar{1}10$] direction. The Si(553)-Pb shows purely one-dimensional bands and band gap in the direction perpendicular to lead nanostructures. Here, metallic bands feature also 1D character, however in the perpendicular direction the band gap is relatively small (in the range of 15 ± 5 meV). Another difference is the symmetry of the surface. The Brillouin

zone of Si(110) has rectangular shape contrary to squeezed hexagons on Si(553). While in the later case it was possible to indicate the origin of each band the same cannot be done for the Si(110)-Pb. The calculated contribution of different lead atoms to the electronic structure is similar which suggests strong interaction between them and the formation of 1D nearly free electron gas. A pair of purely 1D bands observed for Si(110)-Pb resembles electronic structure of gold chains formed on the Si(110) [34] or other silicon vicinal surfaces, in particular Si(553)-Au [20–26].

One of the most commonly used methods for growing one-dimensional (1D) nanostructures is templated self-organization on stepped silicon surfaces. On the other hand similar 1D growth is possible also on surfaces with rectangular symmetry for example Si(110). However, among reported cases of superstructures induced by the presence of: Bi [58], Pt [35,36], Tl [59], Sb [60], Ag [61] atoms, only gold induced 5×2 reconstruction was proven to show 1D metallic bands in electronic structure [33,34]. Finally, it is worth mentioning that the Si(110)-Au was believed to be the most ideal 1D metallic system on low index silicon samples [34]. The results shown in this paper allow us to add the case of Si(110)-Pb to that extremely short list.

V. CONCLUSIONS

In conclusion, we have studied a regular array of hut-shaped lead nanowires on the Si(110) surface. STM images show ordered lead nanostructures running along the [$\bar{1}10$] direction that is unique on the Si(110). The width of nanowires is commensurate with $\times 3$ silicon lattice constant in the [001] direction. The electronic structure shows one-dimensional, parabolic bands crossing the Fermi level in the direction parallel to lead nanowires and small band gap in the perpendicular direction. We propose four different structural models employing different numbers of lead atoms per (1×3) unit cell. The calculated electronic structure fits well the measured data if we take into account that ARPES maps show superposition of bands originating from lead wires with different morphology.

[1] M. Jałochowski and E. Bauer, Quantum size and surface effects in the electrical resistivity and high-energy electron reflectivity of ultrathin lead films, Phys. Rev. B **38**, 5272 (1988).

[2] H. H. Weitering, D. R. Heslinga, and T. Hibma, Structure and growth of epitaxial Pb on Si(111), Phys. Rev. B **45**, 5991 (1992).

[3] M. Hupalo, J. Schmalian, and M. C. Tringides, Devil's Staircase in Pb/Si(111) Ordered Phases, Phys. Rev. Lett. **90**, 216106 (2003).

[4] M. Yakes, V. Yeh, M. Hupalo, and M. C. Tringides, Self-organization at finite temperatures of the devil's staircase in Pb/Si(111), Phys. Rev. B **69**, 224103 (2004).

[5] W. H. Choi, H. Koh, E. Rotenberg, and H. W. Yeom, Electronic structure of dense Pb overlayers on Si(111) investigated using angle-resolved photoemission, Phys. Rev. B **75**, 075329 (2007).

[6] M. Hupalo, S. Kremmer, V. Yeh, L. Berbil-Bautista, E. Abram, and M. Tringides, Uniform island height selection in the low temperature growth of Pb/Si(111)-(7×7), Surf. Sci. **493**, 526 (2001).

[7] M. C. Tringides, M. Jałochowski, and E. Bauer, Quantum size effects in metallic nanostructures, Phys. Today **60**, 50 (2007).

[8] M. T. Hershberger, M. Hupalo, P. A. Thiel, C. Z. Wang, K. M. Ho, and M. C. Tringides, Nonclassical "Explosive" Nucleation in Pb/Si(111) at Low Temperatures, Phys. Rev. Lett. **113**, 236101 (2014).

[9] C. Tegenkamp, Z. Kallassy, H. Pfnür, H.-L. Günter, V. Zielasek, and M. Henzler, Switching Between One and Two Dimensions: Conductivity of Pb-Induced Chain Structures on Si(557), Phys. Rev. Lett. **95**, 176804 (2005).

[10] C. Tegenkamp and H. Pfnür, Switching between one- and two-dimensional conductance: Coupled chains in the monolayer of Pb on Si(557), Surf. Sci. **601**, 2641 (2007).

[11] K. S. Kim, H. Morikawa, W. H. Choi, and H. W. Yeom, Strong Lateral Electron Coupling of Pb Nanowires on Stepped Si(111): Angle-Resolved Photoemission Studies, Phys. Rev. Lett. **99**, 196804 (2007).

[12] C. Tegenkamp, T. Ohta, J. L. McChesney, H. Dil, E. Rotenberg, H. Pfnür, and K. Horn, Coupled Pb Chains on Si(557): Origin of One-Dimensional Conductance, Phys. Rev. Lett. **100**, 076802 (2008).

[13] C. Tegenkamp, D. Lükermann, H. Pfnür, B. Slomski, G. Landolt, and J. H. Dil, Fermi Nesting between Atomic Wires with Strong Spin-Orbit Coupling, Phys. Rev. Lett. **109**, 266401 (2012).

[14] M. Kopciuszyński, P. Dyniec, M. Krawiec, P. Łukasik, M. Jałochowski, and R. Zdyb, Pb nanoribbons on the Si(553) surface, Phys. Rev. B **88**, 155431 (2013).

[15] M. Kopciuszyński, M. Krawiec, R. Zdyb, and M. Jałochowski, Purely one-dimensional bands with a giant spin-orbit splitting: Pb nanoribbons on Si(553) surface, Sci. Rep. **7**, 46215 (2017).

[16] R. Zhao, C. Hu, and W. Yang, Interfacial reaction and surface structures of the Pb/Si(113) system, Surf. Rev. Lett. **2**, 245 (1995).

[17] L. Żurawek, M. Kopciuszyński, M. Dachniewicz, M. Stróżak, M. Krawiec, M. Jałochowski, and R. Zdyb, Partially embedded Pb chains on a vicinal Si(113) surface, Phys. Rev. B **101**, 195434 (2020).

[18] M. Jałochowski and E. Bauer, Growth of metallic nanowires on anisotropic Si substrates: Pb on vicinal Si(001), Si(755), Si(533), and Si(110), Surf. Sci. **480**, 109 (2001).

[19] R. Zdyb, M. Strozak, and M. Jałochowski, Gold-induced faceting on Si(533) surface studied by RHEED, Vacuum **63**, 107 (2001).

[20] J. N. Crain, J. L. McChesney, F. Zheng, M. C. Gallagher, P. C. Snijders, M. Bissen, C. Gundelach, S. C. Erwin, and F. J. Himpsel, Chains of gold atoms with tailored electronic states, Phys. Rev. B **69**, 125401 (2004).

[21] J. R. Ahn, P. G. Kang, K. D. Ryang, and H. W. Yeom, Coexistence of Two Different Peierls Distortions within an Atomic Scale Wire: Si(553)-Au, Phys. Rev. Lett. **95**, 196402 (2005).

[22] I. Barke, F. Zheng, T. K. Rügheimer, and F. J. Himpsel, Experimental Evidence for Spin-Split Bands in a One-Dimensional Chain Structure, Phys. Rev. Lett. **97**, 226405 (2006).

[23] M. Krawiec, Structural model of the Au-induced Si(553) surface: Double Au rows, Phys. Rev. B **81**, 115436 (2010).

[24] J. Aulbach, J. Schäfer, S. C. Erwin, S. Meyer, C. Loho, J. Settelein, and R. Claessen, Evidence for Long-Range Spin Order Instead of a Peierls Transition in Si(553)-Au Chains, Phys. Rev. Lett. **111**, 137203 (2013).

[25] H. W. Yeom, S. W. Jung, J. S. Shin, J. Kim, K. S. Kim, K. Miyamoto, T. Okuda, H. Namatame, A. Kimura, and M. Taniguchi, Direct observation of the spin polarization in Au atomic wires on Si(553), New J. Phys. **16**, 093030 (2014).

[26] M. Krawiec, M. Kopciuszyński, and R. Zdyb, Different spin textures in one-dimensional electronic bands on Si(553)-Au surface, Appl. Surf. Sci. **373**, 26 (2016).

[27] M. Jałochowski, M. Stróżak, and R. Zdyb, Gold-induced ordering on vicinal Si(111), Surf. Sci. **375**, 203 (1997).

[28] K. Altmann, J. Crain, A. Kirakosian, J.-L. Lin, D. Petrovykh, F. Himpsel, and R. Losio, Electronic structure of atomic chains on vicinal Si(111)-Au, Phys. Rev. B **64**, 035406 (2001).

[29] T. Okuda, K. Miyamoto, Y. Takeichi, H. Miyahara, M. Ogawa, A. Harasawa, A. Kimura, I. Matsuda, A. Kakizaki, T. Shishidou, and T. Oguchi, Large out-of-plane spin polarization in a spin-splitting one-dimensional metallic surface state on Si(557)-Au, Phys. Rev. B **82**, 161410(R) (2010).

[30] C. Braun, C. Hogan, S. Chandola, N. Esser, S. Sanna, and W. G. Schmidt, Si(775)-Au atomic chains: Geometry, optical properties, and spin order, Phys. Rev. Mater. **1**, 055002 (2017).

[31] J. L. McChesney, J. N. Crain, V. Pérez-Dieste, F. Zheng, M. C. Gallagher, M. Bissen, C. Gundelach, and F. J. Himpsel, Electronic stabilization of a 5×4 dopant superlattice on Si(111)5×2-Au, Phys. Rev. B **70**, 195430 (2004).

[32] W. H. Choi, P. G. Kang, K. D. Ryang, and H. W. Yeom, Band-Structure Engineering of Gold Atomic Wires on Silicon by Controlled Doping, Phys. Rev. Lett. **100**, 126801 (2008).

[33] J. L. McChesney, J. N. Crain, F. J. Himpsel, and R. Bennewitz, Si(110)5×2-Au: A metallic chain structure, Phys. Rev. B **72**, 035446 (2005).

[34] S. H. Kang, K. S. Kim, and H. W. Yeom, Electronic structure of Au-induced surface phases on Si(110): LEED and angle-resolved photoemission measurements, Phys. Rev. B **78**, 075315 (2008).

[35] A. Visikovskiy, M. Yoshimura, and K. Ueda, Pt-induced structures on Si(110) studied by STM, Appl. Surf. Sci. **254**, 7626 (2008).

[36] J. Park, S. W. Jung, M.-C. Jung, H. Yamane, N. Kosugi, and H. W. Yeom, Self-Assembled Nanowires with Giant Rashba Split Bands, Phys. Rev. Lett. **110**, 036801 (2013).

[37] H. Oyama and T. Ichikawa, Structural study of reconstructions at Si(110)-Pb surfaces, Surf. Sci. **357-358**, 476 (1996).

[38] Y. Kim, J. Ahn, E. Cho, K.-S. An, H. Yeom, H. Koh, E. Rotenberg, and C. Park, Order-disorder phase transition on the Pb-adsorbed Si(110) surface, Surf. Sci. **596**, L325 (2005).

[39] M. Jałochowski and E. Bauer, Reflection high-energy electron diffraction intensity oscillations during the growth of Pb on Si(111), J. Appl. Phys. **63**, 4501 (1988).

[40] M. Kopciuszyński, R. Zdyb, P. Nita, M. Dachniewicz, and P. Dyniec, Quasi one-dimensional lead ribbons on the Si(110) surface, Appl. Surf. Sci. **373**, 8 (2016).

[41] J. P. Perdew, K. Burke, and M. Ernzerhof, Generalized Gradient Approximation Made Simple, Phys. Rev. Lett. **77**, 3865 (1996).

[42] G. Kresse and J. Furthmüller, Efficient iterative schemes for ab initio total-energy calculations using a plane-wave basis set, Phys. Rev. B **54**, 11169 (1996).

[43] G. Kresse and D. Joubert, From ultrasoft pseudopotentials to the projector augmented-wave method, Phys. Rev. B **59**, 1758 (1999).

[44] P. E. Blöchl, Projector augmented-wave method, Phys. Rev. B **50**, 17953 (1994).

[45] H. J. Monkhorst and J. D. Pack, Special points for Brillouin-zone integrations, Phys. Rev. B **13**, 5188 (1976).

[46] K. Sakamoto, M. Setvin, K. Mawatari, P. E. J. Eriksson, K. Miki, and R. I. G. Uhrberg, Electronic structure of the Si(110)-(16×2) surface: High-resolution ARPES and STM investigation, Phys. Rev. B **79**, 045304 (2009).

[47] N. K. Lewis, N. B. Clayburn, E. Brunkow, T. J. Gay, Y. Lassailly, J. Fujii, I. Vobornik, W. R. Flavell, and E. A. Seddon, Domain formation mechanism of the Si(110) "16×2" reconstruction, Phys. Rev. B **95**, 205306 (2017).

[48] M. Kisiel, K. Skrobas, and M. Jałochowski, Angle-resolved photoemission of ultrathin Pb films on Si(111)-(6×6)Au: quantum size effect, Optica Applicata **35**, 443 (2005).

[49] B. Slomski, F. Meier, J. Osterwalder, and J. H. Dil, Controlling the effective mass of quantum well states in pb/si(111) by interface engineering, Phys. Rev. B **83**, 035409 (2011).

[50] M. Jałochowski, K. Palotás, and M. Krawiec, Spilling of electronic states in Pb quantum wells, Phys. Rev. B **93**, 035437 (2016).

[51] Y. A. Bychkov and E. I. Rashba, Oscillatory effects and the magnetic susceptibility of carriers in inversion layers, J. Phys. C: Solid State Phys. **17**, 6039 (1984).

[52] M. Czubanowski, A. Schuster, S. Akbari, H. Pfnür, and C. Tegenkamp, Adsorbate induced refacetting: Pb chains on Si(557), New J. Phys. **9**, 338 (2007).

[53] M. Kopciuszyński, P. Łukasik, R. Zdyb, and M. Jałochowski, Ordering of the Si(553) surface with Pb atoms, Appl. Surf. Sci. **305**, 139 (2014).

[54] H. Morikawa, K. S. Kim, D. Y. Jung, and H. W. Yeom, Scanning tunneling microscopy observation of Pb-induced superstructures on Si(557), Phys. Rev. B **76**, 165406 (2007).

[55] H. Pfnür, C. Brand, M. Jäger, J. Rönspies, and C. Tegenkamp, Between one and two dimensions: Pb/Si(557) close to monolayer coverage, Surf. Sci. **643**, 79 (2016).

[56] T. Zhang, P. Cheng, W.-J. Li, Y.-J. Sun, G. Wang, X.-G. Zhu, K. He, L. Wang, X. Ma, X. Chen, Y. Wang, Y. Liu, H.-Q. Lin, J.-F. Jia, and Q.-K. Xue, Superconductivity in one-atomic-layer metal films grown on Si(111), Nat. Phys. **6**, 104 (2010).

[57] M. Yamada, T. Hirahara, and S. Hasegawa, Magnetoresistance Measurements of a Superconducting Surface State of In-Induced and Pb-Induced Structures on si(111), Phys. Rev. Lett. **110**, 237001 (2013).

[58] A. K. R. Ang, S. N. Takeda, and H. Daimon, Bi induced superstructures on Si(110), J. Vac. Sci. Technol. A **34**, 051401 (2016).

[59] E. Annese, T. Kuzumaki, B. Müller, Y. Yamamoto, H. Nakano, H. Kato, A. Araki, M. Ohtaka, T. Aoki, H. Ishikawa *et al.*, Nonvortical Rashba Spin Structure on a Surface with C1h Symmetry, Phys. Rev. Lett. **117**, 016803 (2016).

[60] A. Cricenti, P. Perfetti, G. Le Lay, J. Zeysing, G. Falkenberg, L. Seehofer, and R. L. Johnson, Sb/Si(110) 2×3 surface studied with scanning tunneling microscopy: Evidence for adatom reconstruction, Phys. Rev. B **60**, 13280 (1999).

[61] N. Maslova, A. Oreshkin, S. Oreshkin, V. Panov, I. Radchenko, and S. Savinov, Ag-induced atomic structures on the Si(110) surface, JETP Lett. **84**, 320 (2006).